Ab initio investigation of the adsorption of phenolic compounds, CO, and H 2 O over metallic cluster/silica catalysts for hydrodeoxygenation process

Saber Gueddida, Sébastien Lebègue, Andreea Pasc, Anthony Dufour, Michael Badawi

Ab initio investigation of the adsorption of phenolic compounds, CO, and H_2O over metallic cluster/silica catalysts for hydrodeoxygenation process

Saber Gueddida[a,*], Sébastien Lebègue[a], Andreea Pasc[b], Anthony Dufour[c], Michael Badawi[a,*]

[a] *Lorraine University, Laboratoire de Physique et Chimie Théoriques, CNRS:UMR-7019, Vandoeuvre-lès-Nancy 54506, France.*
[b] *Lorraine University, MolSyBio, L2CM, CNRS UMR7053, F-54506 Vandoeuvre-Les-Nancy, France.*
[c] *Lorraine University, LRGP, CNRS, ENSIC, 54000 Nancy, France.*

Abstract

The catalytic hydrodeoxygenation (HDO) of lignin is an important route to produce green aromatics. Herein we study the adsorption of key phenolic molecules (phenol, catechol, guaiacol, anisole) over various metallic nanoparticles (NP) (Ni, Cu, Co, Fe) supported over amorphous silica, by the periodic spin polarized density functional theory (DFT). CO and water are potential inhibiting molecules present in the lignin pyrolysis gas. Therefore their competing adsorption is also studied in details. Our calculations show that the oxygenated compounds have a stronger interaction at the interface between the NP cluster and the silica for all the studied metals. By comparing the resulting adsorption energies, we found that the Ni_{13}@silica catalyst is the most attractive one for oxygenated molecules. The most stable configuration is a phenol adsorption at the interface through the OH group with the silica surface and the aromatic ring with the transition metal cluster. In addition, we show that the adsorption of the oxygenated compounds is not impacted by the presence of inhibiting molecules on Fe_{13}@silica, Co_{13}@silica and Ni_{13}@silica catalysts. This type of DFT investigation appears to be useful to suggest suitable formulations for an optimal HDO of lignin.

Keywords: DFT, HDO, guaiacol, transition metal clusters, Amorphous silica surfaces, inhibiting effect.

1. Introduction

Lignin has attracted a tremendous interest to produce green aromatic chemicals [1, 2]. Indeed, it is the most abundant natural macromolecules composed of an aromatic structure.

* *Email addresses:* saber.gueddida@univ-lorraine.fr (Saber Gueddida), michael.badawi@univ-lorraine.fr (Michael Badawi)

Lignin is composed of different phenolic units linked with numerous ether bonds (mainly β-O-4) or C-C bonds [3, 4]. Its high molecular complexity impedes its valorization to high added-value chemicals like aromatics (phenol, benzene or p-xylene) and calls for the development of tailored catalysts and reactors [5]. Technical lignins produced for instance by the Kraft process are even more recalcitrant than native lignins and present mainly C-C bonds between the aromatic units. Pyrolysis can be a versatile technology to convert various lignins into a liquid (bio-oil), a gas and a char [6]. The hydrodeoxygenation (HDO) of lignin bio-oils have been proposed as an interesting strategy to target various aromatic chemicals [7, 8, 9]. Guaiacol has been selected as a key surrogate to mimic lignin pyrolysis vapours in several studies [10, 11, 12]. Phenol is also a key molecule: it can be the targeted molecule to produce lignin-derived green materials but it is also the most refractory key intermediate to produce benzene [9, 13, 14, 15, 16, 17, 18]. Theoretical and experimental studies show that phenolic compounds can follow two main deoxygenation routes: (1) hydrogenation of the phenyl ring into cyclohexyl before a C-O bond cleavage denoted hydrogenation (HYD) route or (2) direct cleavage of the C-O bond denoted direct deoxygenation (DDO) route [19, 20, 21, 22, 23, 24]. The DDO is the prefered reaction in order to reduce hydrogen consumption and to produce green aromatics (like benzene, xylenes or phenols). The presence of phenolic compounds such as ethers could lead to the formation of CO via the reduction of CO_2 [25, 19]. Furthermore H_2O molecules are also exist under HDO conditions [25, 19]. These compounds may affect the reactivity of oxygenated molecules by competition for adsorption.

Several type of catalysts have been used for HDO processing, including metal sulfides such (Co, Ni)-MoS_2 and oxophilic supports such as ZrO_2, TiO_2, Nb_2O_5 [26, 27, 28, 20, 29, 30, 25, 31, 32, 33] which are selective to produce aromatics via the DDO route [34, 35, 20]. Noble metals such as Pd, Pt and Rh are particularly efficient in HDO, however they are expensive and not selective for the DDO route by promoting the hydrogenation of the aromatic cycles [28, 33]. The competition between the HYD and DDO pathways within non-noble metals (iron and cobalt) has been studied by Olcese *et al.* [10, 11, 9]. They showed that Fe@silica has an interesting selectivity to the DDO pathway. On the other hand, a promising performance has been shown for silica catalysts in the HDO process that favors the DDO pathway and supports the lowest inhibitory effect of the by-products [19, 36]. Silica-based materials are also among the most common supports due to their specific physico-chemical properties such as mechanical resistance, high dielectric strength, and ease of chemical modification [37, 38, 39, 40, 41], abundance and low cost [42, 43, 44]. In particular, porous silica materials containing metallic nanoparticles such as iron, cobalt, nickel or copper are attractive for many catalytic applications like hydrodeoxygenation [45, 46, 47, 48].

Recently, using theoretical approachs, Gueddida *et al.* [49, 50] have rationalized the different grafting mechanism of several transition metal species (isolated ions or clusters) onto various silica surfaces. The chosen clusters are of 13 atoms (symmetry of D_{3d}) because it exhibits a high dynamic stability and corresponds to the size of experimentally transition metal nanoparticles observed on SBA-15 [45, 46]. The models were in agreement with the experimental findings and showed that Ni clusters are the most energetically stable compared to the Fe, Co, and Cu ones, which could be further used to optimize the design of catalytic nanomaterials with improved activity and selectivity. Herein, a better understanding of the

interaction mode of the oxygenated compounds as well as the inhibiting molecules over pure and supported silica catalysts will provide to improve the DDO pathway. Therefore, the goal of this study is to elucidate the adsorption mechanisms and to evaluate the adsorption energies of phenolic molecules and of some by-products (H_2O, CO) over pristine and Fe, Co, Ni, Cu-supported clusters onto silica. This study enables to improve our understanding of HDO fundamentals and therefore to design tailored catalysts for green aromatics production from lignin.

2. Calculation details

Our density functional theory simulations were conducted using the VASP-5.4 code [51]. The PAW method [52] has been used and the cutoff energy set to 450 eV. The exchange-correlation potential was accounted using the formulation of Perdew, Burke, and Ernzerhof (PBE) [53], associated with the dispersion correction scheme of Grimme [54, 55]. In order to describe correctly the $3d$-states in transition metals which tends to be inaccurately represented in the PBE functional, we used the rotationally invariant PBE+U correction [56, 57], as available in the VASP code. The values of the Hubbard parameters U and J are fixed to 3 eV and 0.9 eV, respectively, for all the systems containing d-metals [49, 50]. These parameters are adopted in order to reproduce the structural, electronic and magnetic properties of the transition metal clusters available in the literature [58, 59, 60, 61, 62].

Earlier theoretical calculations within PBE+U+D2 approximation have been realized to found the most favorable configurations of the heterogeneous M_{13}@silica catalysts [49, 50]. It has been shown that a silanol density of 3.3 OH·nm^{-2} is typical for an experimental situation that follows various synthesis pathways of mesoporous silica under vacuum conditions at 200°C [63, 64, 65, 66, 67, 36]. Gueddida *et al.* have also studied theoretically the different grafting modes for iron, cobalt, nickel, and copper clusters on the silica-3.3 surface [49, 50] and they have shown that are energetically stable. Therefore, herein, we used the amorphous silica substrate with a density of silanol equal to 3.3 OH·nm^{-2} [68], whose supercell consists of 227 oxygen, 102 silicon and 46 hydrogen atoms.

In all considered systems, a vacuum of 20 Å in the z direction was used to separate the periodic super cells. The lattice parameters of these systems are a = 21.39 Å, b = 21.39 Å, c = 34.17 Å, α=90°, β=90° and γ=90° [68]. Due to the large size of the super cells, we used only the Γ point to sample the first Brillouin zone. The convergence threshold on the difference of the Kohn Sham self-consistent total energy are set to 10^{-6}eV. For the geometry optimization, the positions of all atoms of guaiacol, catechol, anisole, phenol, CO, H_2O, transition metal clusters and the first layer of the silica surface were allowed to relax while keeping the other planes frozen. The force criterion for relaxation was fixed to 0.03 eV/Å.

3. Results

In order to find the best adsorption configurations of the phenolic compounds and potential molecules (H_2O, CO) onto pure silica surface or supported transition metal clusters (Fe_{13}, Co_{13}, Ni_{13}, or Cu_{13}@silica), we have undertaken a systematic investigation of possible

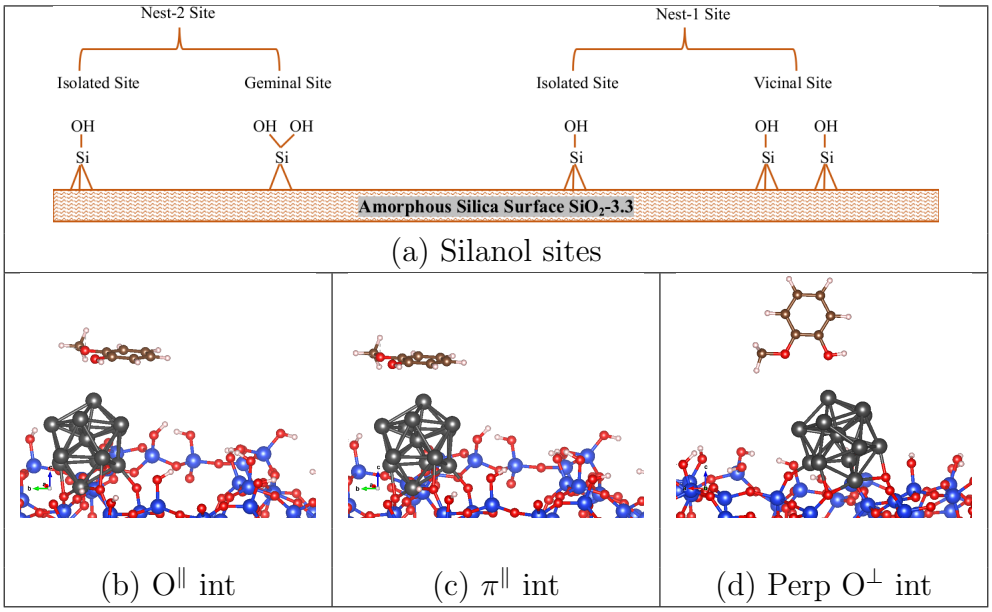

Figure 1: (a): Different silanol sites existing on the amorphous silica surface (SiO_2-3.3): geminal, vicinal, isolated, nest-1 and nest-2. (b, c, and d): Interactions modes for guaiacol molecule on the top of metallic clusters of M_{13}@silica materials: M = (Fe, Co, Ni, and Cu) atoms in dark-gray, C atoms in brown, O atoms in red, Si atoms in blue, and H atoms in white. (b) flat adsorption through oxygenated group of guaiacol, (c) flat adsorption through aromatic ring, and (d) perpendicular adsorption through oxygenated group.

cases with regard to the location of the molecule on the material as well as molecule orientations. For example, for the phenol adsorption, up to 48 possible configurations have been tested (see Figure S1 in Supporting Information). For all cases, three adsorption modes (see Figure 1) have been investigated: the perpendicular and the flat O interaction modes ($O^{\perp}$ and $O^{\parallel}$, respectively) where the interaction of the phenolic molecule to the surface is established through its oxygen atom. For the $O^{\parallel}$ mode, the considered molecule can interact also with the support via its aromatic ring (when the parallel aromatic ring is close enough to the support). The flat π interaction mode ($\pi^{\parallel}$) is induced mainly by the interaction between the aromatic ring and the support.

3.1. Pure silica surface

The computed interaction energies between the most favorable structures of the phenolic compounds or potential inhibiting molecules and the different silanol groups (nest-1, isolated, vicinal, geminal, nest-2) of the silica-3.3 surface are summarized in Table 1. The adsorption energy ΔE_1 is given by $\Delta E_1 = E_{TotSys} - E_{mol} - E_{surf}$, where E_{TotSys}, E_{mol} and E_{surf} are the PBE+D2 total energies of the (molecule+surface) system, the isolated molecule and the surface alone, respectively.

Our calculations show that the phenolic compounds are strongly connected to the silanol group nest-1 through a $O^{\parallel}$ mode with ΔE_1 equal to -306 kJ·mol^{-1} for guaiacol, -325 kJ·mol^{-1} for catechol, -115 kJ·mol^{-1} for anisole, and -115 kJ·mol^{-1} for phenol. A significant adsorption energy is also observed for guaiacol via the $O^{\parallel}$ mode, where the isolated and the vicinal

Table 1: PBE+D2 computed adsorption energies (in kJ·mol^{-1}) for the most stable structures of the phenolic compounds and the inhibiting molecules onto amorphous silica surface silica-3.3 at the different silanol groups (nest-1, isolated, vicinal, geminal, nest-2).

Molecule	Interaction mode	Silanol sites				
		Isolated	Nest-1	Vicinal	Nest-2	Geminal
Guaiacol	$O^{\perp}$	-48	-56	-56	-46	-32
	$O^{\parallel}$	-75	**-306**	-75	-64	-56
	$\pi^{\parallel}$	-47	-51	-62	-44	-42
Catechol	$O^{\perp}$	-40	-49	-54	-38	-24
	$O^{\parallel}$	-54	**-325**	-73	-64	-54
	$\pi^{\parallel}$	-39	-43	-51	-71	-35
Anisole	$O^{\perp}$	-41	-33	-42	-42	-5
	$O^{\parallel}$	52	**-115**	-38	-53	-44
	$\pi^{\parallel}$	-44	-42	-44	-37	-41
Phenol[19, 71]	$O^{\perp}$	-34	-54	-20	-73	-23
	$O^{\parallel}$	-31	**-117**	-35	-77	-24
	$\pi^{\parallel}$	-29	-33	-18	-42	-22
CO[19, 71]		-11	-11	-11	-12	-7
H_2O[19, 71]		-34	-51	-24	-70	-19

sites coexist with an adsorption energy of -75 kJ·mol^{-1}, and the vicinal and the nest-2 sites for catechol with ΔE_1 of -73 kJ·mol^{-1} and -71 kJ·mol^{-1} via $O^{\parallel}$ and $\pi^{\parallel}$ modes, respectively. The adsorption energies of the anisole molecule on the isolated and the nest-2 sites via the $O^{\parallel}$ mode are very similar (-52 kJ·mol^{-1} and -53 kJ·mol^{-1}, respectively). For the phenol molecule, we found that the $O^{\perp}$ and $O^{\parallel}$ interaction modes coexist on the nest-2 adsorption silanol group with ΔE_1 equal to -73 kJ·mol^{-1} and -77 kJ·mol^{-1}, respectively. For all silanol adsorption groups, our results show that the phenolic compounds prefer mainly the adsorption via the $O^{\parallel}$ interaction mode, while the $O^{\perp}$ and the $\pi^{\parallel}$ modes present similar energy values. The adsorption of CO on various silanol groups is not favorable (about -10 kJ·mol^{-1}), while H_2O present significant adsorption energies on the nest-1 and 2 groups of -51 kJ·mol^{-1} and -70 kJ·mol^{-1}, respectively. Therefore, the adsorption of the phenolic compounds is not impacted by the presence of the inhibiting molecules (CO and H_2O) over the pristine silica.

The larger ΔE_1 energy of the phenolic compounds on the silanol site nest-1 is due to the strong interaction of the aromatic ring (C_5 or C_4) to one silica atom of the surface (labelled here as Si_{52}) leading to a distortion of its aromatic ring. In addition, the adsorption of the guaiacol or catechol modify the surface state of the amorphous silica: it breaks one Si_3-O_{196}-Si_{52} bond and releases a hydrogen atom from one of its hydroxyl groups (for the nomenclature

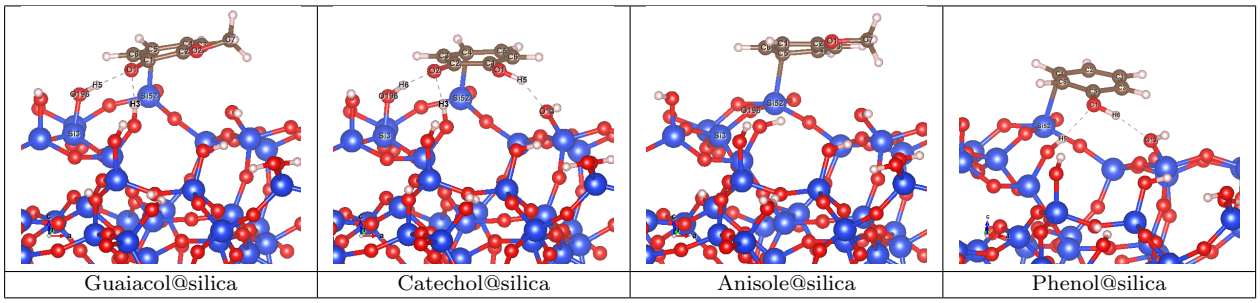

Figure 2: The most stable structures of guaiacol, catechol, anisole, and phenol molecules adsorbed onto pure silica-3.3 surface: O atoms in red, Si atoms in blue, and H atoms in white.

of the molecule see Figure 2), generating new silanol sites, $Si_3O_{196}H_5$ for guaiacol@silica and $Si_3O_{196}H_6$ for catechol@silica. These particular stable adsorption structures of the guaiacol molecule and its derivatives onto the amorphous silica surface are shown in Figure 2. For the guaiacol@silica system, our calculations show the formation of 2 O$\cdots$H bonds between O_1 of its broken hydroxyl group of guaiacol and H_3 of the vicinal silanol group and the second with the hydrogen atom of a new silanol ($Si_3O_{196}H_5$) group with a distance of 1.67 Å. However, the interaction of the catechol molecule to the silica surface is established by the formation of three O$\cdots$H bonds: two hydrogen bonds similar to the guaiacol molecule with distances of 1.70 and 1.55 Å, respectively, and one O$\cdots$H bond between H_5 of the hydroxyl group of catechol and O_{13} of the silanol group with a distance of 1.74 Å. Two O$\cdots$H bonds are established for phenol@silica: one between H_6 of the hydroxyl group and O_{13} of the silanol group with a distance of 1.75 Å and the second between O_1 of the phenol and H_5 of the surface with a distance of 1.93 Å, while no hydrogen bonds are established for anisole. On the other hand, the oxygenated compounds are strongly connected to the surface via a strong interaction between the carbon of the aromatic ring (C_4 or C_5) and the interfacial silicon atom (Si_{52}) of 1.99 Å for guaiacol and catechol, 2.08 Å for anisole, and 2.32 Å for phenol.

These are in agreement with the infrared results of Rochester *et al.* [69] which have shown that there are two types of surface-adsorbate interaction, one involving the formation of hydrogen bonds between surface silanol groups and the aromatic π-electron systems of adsorbed phenolic molecules, and the other involving hydrogen bonds between silanol groups and the phenolic hydroxy groups of adsorbed species. Besides, Popov *et al.* [70] have shown that phenol, anisole, and guaiacol mainly interact with silica via H-bonding.

3.2. Heterogeneous catalysts

3.2.1. Adsorption of oxygenated species

Energetics. The adsorption energy ΔE_2 of the phenolic compounds, or the inhibiting molecules on the heterogeneous catalysts was computed as $\Delta E_2 = E_{Molecule/M_{13}@SiO_2} - E_{Molecule} - E_{M_{13}@SiO_2}$ were $E_{Molecule/M_{13}@SiO_2}$, $E_{Molecule}$, $E_{M_{13}@SiO_2}$ are the PBE+U+D2 total energy of the adsorbed guaiacol, catechol, anisole, phenol, CO, or H_2O molecule onto M_{13}@silica catalysts, of the isolated gas phase molecule (guaiacol, catechol, anisole, phenol, CO, or H_2O) and of the free M_{13}@silica systems.

Our computed adsorption energies for different adsorption structures are displayed in Table 2. Our calculations show that the considered molecules are weakly adsorbed (around

Table 2: Calculated ΔE_2 (in kJ·mol^{-1}) for all adsorption structures of phenolic compounds onto the heterogeneous catalysts (M_{13} cluster and M_{13}@silica interface) using the PBE+U+D2 approximation.

Heterogeneous catalysts	Molecule	Cluster M_{13}		Interface M_{13}@silica	
		$O^{\perp}$	$\pi^{\parallel}$	$O^{\parallel}$	$\pi^{\parallel}$
Fe_{13}@silica	Guaiacol	-14	-95	-126	**-219**
	Catechol	-24	-89	-190	**-218**
	Anisole	-13	-95	-112	**-228**
	Phenol	-43	-87	-117	**-247**
Co_{13}@silica	Guaiacol	-15	-129	-131	**-225**
	Catechol	-16	-120	-197	**-216**
	Anisole	-15	-127	-124	**-230**
	Phenol	-40	-119	-108	**-264**
Ni_{13}@silica	Guaiacol	-19	-126	-145	**-284**
	Catechol	-36	-121	-185	**-284**
	Anisole	-17	-123	-199	**-288**
	Phenol	-63	-113	-276	**-295**
Cu_{13}@silica	Guaiacol	-14	-76	-144	**-201**
	Catechol	-14	-70	-146	**-157**
	Anisole	-14	-69	-164	**-190**
	Phenol	-24	-64	-95	**-221**

-15 kJ·mol^{-1}) on the transition metal clusters via $O^{\perp}$ mode except for the phenol molecule on (Fe_{13}, Co_{13}, and Ni_{13})@silica with values of -43 kJ·mol^{-1}, -40 kJ·mol^{-1}, and -63 kJ·mol^{-1}, respectively. However, these molecules are strongly adsorbed on the top of the M_{13} cluster through a $\pi^{\parallel}$ mode with ΔE_2 in the range of [-87, -95] kJ·mol^{-1} for Fe_{13}@silica, [-119, -129] kJ·mol^{-1} for Co_{13}@silica, [-113, -126] kJ·mol^{-1} for Ni_{13}@silica, and [-64, -76] kJ·mol^{-1} for Cu_{13}@silica. We found that the interactions between the phenolic compounds and Co_{13} or Ni_{13} clusters are stronger than those with Fe_{13} and less than with Cu_{13} one. The adsorption of the guaiacol and the anisole molecules on the top of the different transition metal cluster via the $\pi^{\parallel}$ mode are slightly more stable than those of the catechol and the phenol molecules.

Also, our calculations show that the adsorption of the phenolic compounds at the interface M_{13}@silica through both $O^{\parallel}$ and $\pi^{\parallel}$ modes are more favorable than that on the transition metal clusters. For Fe_{13}@silica, the resulting adsorption energies of guaiacol, catechol, anisole, and phenol via $\pi^{\parallel}$ mode are, respectively, 93, 28, 116, and 130 kJ·mol^{-1} higher than those through $O^{\parallel}$ mode, while for Co_{13}@silica, are 94, 19, 106, and 156 kJ·mol^{-1}, respectively. These molecules favor the adsorption via the $\pi^{\parallel}$ mode rather than the $O^{\parallel}$ one with an energy difference of 139, 99, 89, and 19 kJ·mol^{-1} for (guaiacol, catechol, anisole, and phenol)/Ni_{13}@silica, and 57, 11, 26, and 126 kJ·mol^{-1} for those adsorbed on Cu_{13}@silica interface. For all cases, the phenolic compounds is strongly adsorbed at the

interface M_{13}@silica via the $\pi^{\parallel}$ mode. This result is of high importance to understand the catalytic mechanisms of phenolics HDO over metal/silica. It suggests that the main active sites of adsorption would be at the interface between the metallic nanoparticles and the silica support.

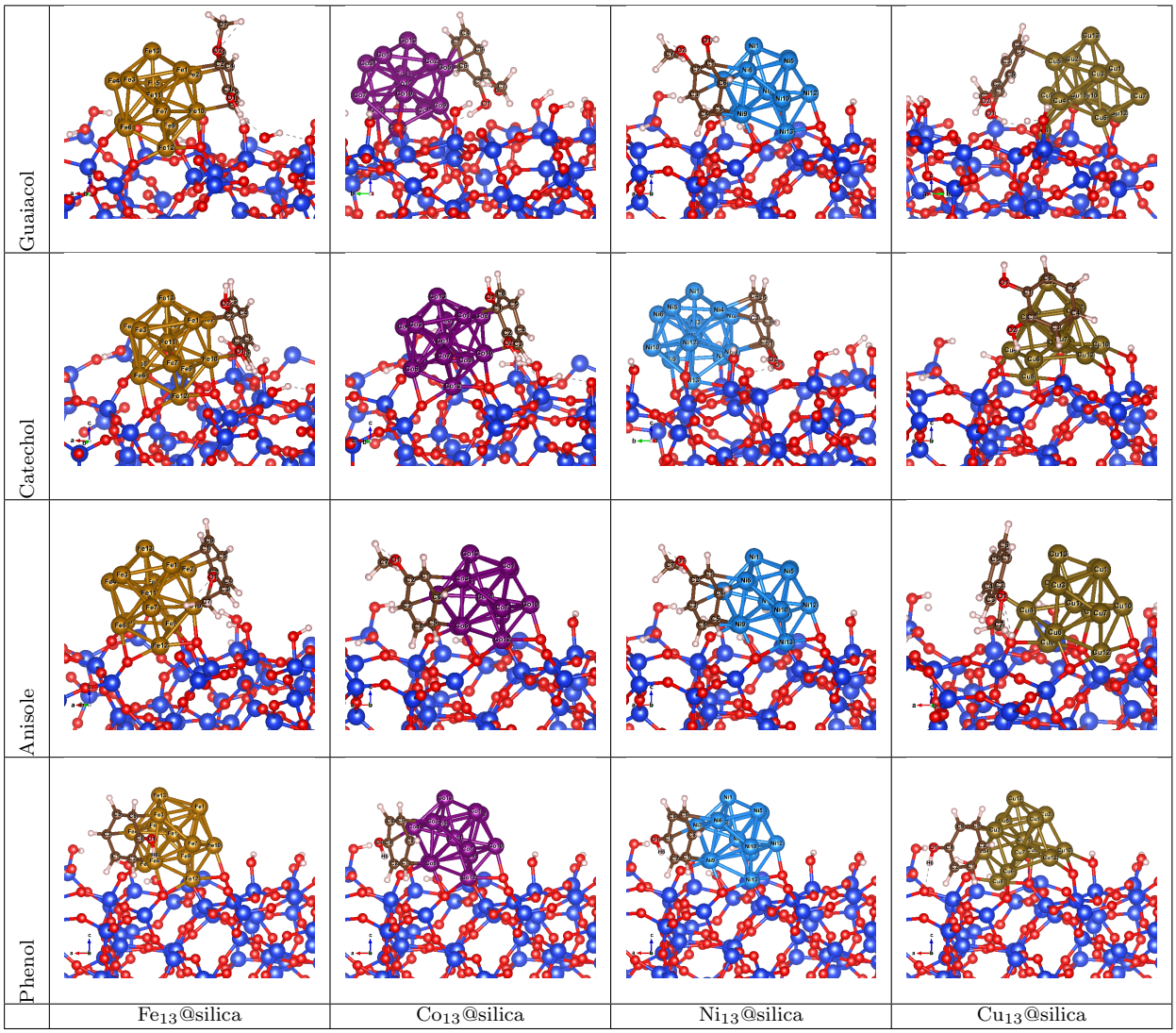

Figure 3: The most stable structures of guaiacol, catechol, anisole, and phenol molecules adsorbed onto different heterogeneous catalysts (Fe_{13}@silica, Co_{13}@silica, Ni_{13}@silica, and Cu_{13}@silica): O atoms in red, Si atoms in blue, and H atoms in white.

Geometries. Figure 3 shows the most favorable structures of the adsorbed guaiacol molecule and its derivatives on different M_{13}@silica catalysts. For guaiacol/M_{13}@silica, the interaction between the guaiacol molecule and the heterogeneous catalysts is established by the formation of M-C bonds between the aromatic ring of the guaiacol molecule and the transition metal cluster, and O$\cdots$H bonds between the hydrogen of the hydroxyl group of

guaiacol and the oxygen of the silanol silica group. Our calculations show that the guaiacol molecule is connected to M_{13} cluster through three M-C bonds for Fe_{13}@silica, four bonds for Co_{13}@silica, six bonds for Ni_{13}@silica, and only one bond is established for Cu_{13}@silica. In addition, for guaiacol/Fe_{13}@silica, guaiacol/Co_{13}@silica, and guaiacol/Cu_{13}@silica, we found that the hydroxyl group of the guaiacol molecule is pointed towards the silica surface and therefore the formation of a O$\cdots$H bond between them with a value of 1.88 Å, 1.42 Å, and 1.71 Å, respectively. More details about the computed bond lengths (d_{C-H}, d_{C-C}, d_{C-O}, and d_{O-H}) and bond angles of the isolated and the interacted guaiacol molecule and the equilibrium interatomic distances between the aromatic ring of the guaiacol molecule and the M_{13} clusters (d_{M-C}), are given in Table S1 (see the Supporting Information). The equilibrium d_{M-C} distances are ranged between 2.07 and 2.13 Å for Fe_{13}@silica, 2.15 and 2.19 Å for Co_{13}@silica, and 2.03 and 2.15 Å for Ni_{13}@silica. However, the Cu-C bond lengths are of 2.23 Å. We found that the interaction of the guaiacol molecule with the different heterogeneous catalysts activate its C-O bonds (more details are given in the Supporting Information).

For catechol/M_{13}@silica, the interaction between the catechol molecule and the heterogeneous catalysts occurs by formation of three M-C bonds for Fe_{13}@silica and Co_{13}@silica, six bonds for Ni_{13}@silica, and two bonds for Cu_{13}@silica and their equilibrium distances are found in the range of 2.06-2.08 Å, 2.02-2.07 Å, 2.02-2.15 Å, and 2.14-2.18 Å, respectively. The catechol molecule is also connected to the different heterogeneous catalysts through one O$\cdots$H bond between the silica surface and the closest hydroxyl group of the molecule with an equilibrium distance of 1.88, 1.93, 1.80, and 1.71 Å for catechol/Fe_{13}@silica, catechol/Co_{13}@silica, catechol/Ni_{13}@silica, and catechol/Cu_{13}@silica, respectively. The computed d_{C-C}, d_{C-O}, and d_{O-H} bond lengths and the different bond angles of the adsorbed catechol molecule are influenced by the interaction with the heterogeneous catalysts compared to those of the free molecule (see Table S2, more details are given in the Supporting Information).

For the anisole molecule, the interaction with the heterogeneous catalysts occurs only by formation of M-C bonds through transition-metal clusters. For the most favorable structures, our calculations show the formation of two M-C bonds for Fe_{13}@silica, four bonds for Co_{13}@silica, six bonds for Ni_{13}@silica, and only one bond for Cu_{13}@silica with a distance value ranged between 2.03 and 2.08 Å, 2.05 and 2.19 Å, 2.04 and 2.11 Å, and 2.27 Å, respectively. By comparing the calculated geometrical parameters of the free and the adsorbed anisole molecule (see Table S3 in the Supporting Information), we found that the interaction of the anisole molecule to the different heterogeneous catalysts have a strong effect on its geometrical structure.

For phenol/M_{13}@silica, the interaction between the phenol molecule and the heterogeneous catalysts occurs by formation of M-C and O$\cdots$H bonds. The optimized structures show the formation of three M-C bonds for phenol/Fe_{13}@silica and four bonds for the phenol/Co_{13}@silica system. For phenol/Ni_{13}@silica, the phenol molecule is connected to the nickel cluster through six M-C bonds. However, for the phenol/Cu_{13}@silica system, only two M-C bonds are established. The Ni-C interatomic distances are ranged between 2.03 and 2.14 Å, while Fe-C and Co-C are in the range of 2.05-2.09 Å and 2.03-2.17 Å, respectively.

The equilibrium distance between phenol and Cu_{13} cluster are ranged from 2.15 to 2.17 Å. The calculations show also the creation of one O$\cdots$H bond between the hydrogen atom of the phenol hydroxyl group and the oxygen atom of the silanol silica group with a distance value of 1.56 Å, 1.70 Å, 1.83 Å, and 2.05 Å for phenol/Fe_{13}@silica, phenol/Co_{13}@silica, phenol/Ni_{13}@silica, and phenol/Cu_{13}@silica systems, respectively.

Our results show that the geometric structures of the phenol molecule is strongly affected (deformation of its aromatic ring) by its interaction with the heterogeneous catalysts (Fe, Co, and Ni), however, the effect is lower when phenol is connected to Cu_{13}@silica. This effect is clearly observed on the interatomic bond lengths d_{C-C}, d_{C-O}, and d_{O-H} and the different bond angles of the phenol molecule. The calculated geometrical parameters of the isolated and the interacted phenol molecule (interatomic bond lengths and bond angles) and the equilibrium distances between the aromatic ring of the phenol molecule and the transition metal clusters (d_{M-C}) are reported in Table S4 (see the Supporting Information with more details).

Table 3: Calculated ΔE_2 (in kJ·mol^{-1}) for all adsorption configurations of the inhibiting molecules onto the heterogeneous catalysts (M_{13} cluster and M_{13}@silica interface) using PBE+U+D2 approximation.

Heterogeneous catalysts	Molecule	Cluster M_{13}	Interface M_{13}@silica
Fe_{13}@silica	CO	-151	-185
	H_2O	-51	-136
Co_{13}@silica	CO	-145	-177
	H_2O	-49	-139
Ni_{13}@silica	CO	-197	-232
	H_2O	-64	-165
Cu_{13}@silica	CO	-85	-191
	H_2O	-43	-150

3.2.2. Inhibiting molecules

Energetics. Table 3 shows the adsorption energies of the potential inhibiting molecules (CO and H_2O) on the top of the transition metal clusters (Fe_{13}, Co_{13}, Ni_{13}, and Cu_{13}) and at their corresponding interfaces with the silica surface. The resulting adsorption energies of the CO molecule on the top of Fe_{13}, Co_{13} and Ni_{13} clusters are -151, -145 and -197 kJ·mol^{-1}, respectively. At the Fe_{13}@silica, Co_{13}@silica and Ni_{13}@silica interfaces, the adsorption energy values are of -185, -177 and -232 kJ·mol^{-1}, respectively, which are always around 30 kJ·mol^{-1} higher in absolute value than the corresponding ones on the metallic clusters only. For water, at the (Fe_{13}, Co_{13} and Ni_{13}@silica) interfaces, ΔE_2 are found to be -136, -139 and -165 kJ·mol^{-1}, which are 85, 90, and 101 kJ·mol^{-1}, respectively, higher than those on the top of the corresponding clusters. However, for Cu_{13}@silica, the adsorption of both molecules at the interface are $\sim$106 kJ·mol^{-1} higher than that on the top of Cu_{13} cluster. For all cases, our results show that the water molecule is in general less adsorbed than the CO one.

Figure 4: The most stable structures of the inhibiting molecules CO (upper panel) and water (lower panel) adsorbed onto different heterogeneous catalysts (Fe_{13}@silica, Co_{13}@silica, Ni_{13}@silica, and Cu_{13}@silica).

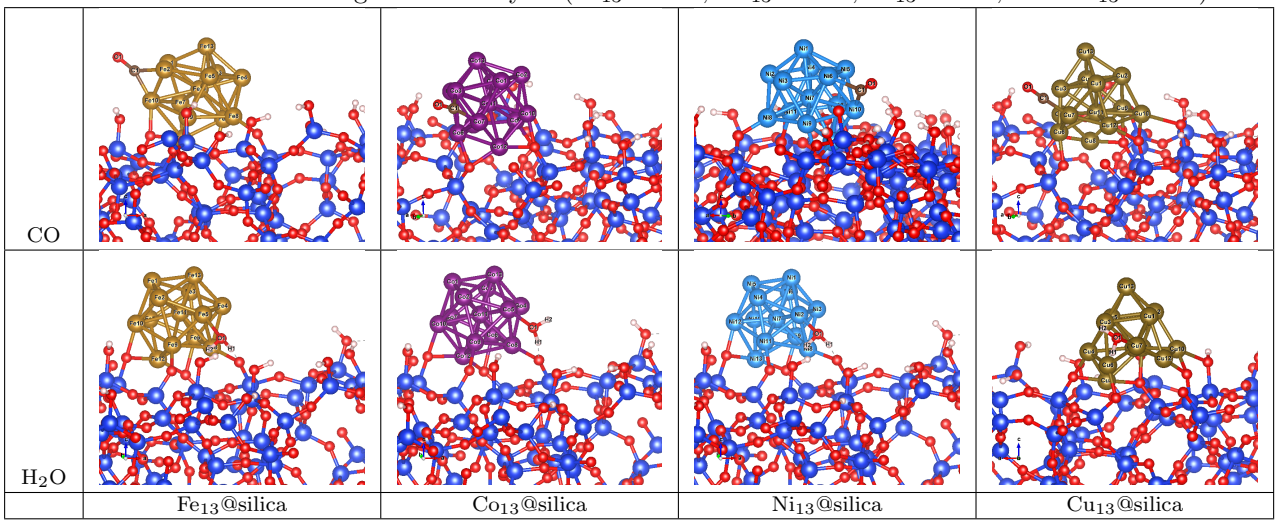

Geometries. Figure 4 shows the most favorable structures of CO and H_2O molecules onto M_{13}@silica. Our calculations show that the CO molecule is connected to the transition metal cluster through two M-C bonds (bridge adsorption) for Fe_{13}@silica, Co_{13}@silica, and Ni_{13}@silica catalysts and only one bond is established for Cu_{13}@silica (top adsorption). The equilibrium distances d_{M-C} between the CO molecule and the transition metal clusters Fe_{13}, Co_{13}, Ni_{13}, and Cu_{13} are found to be 1.91-2.06 Å, 1.80-2.09 Å, 1.79-1.94 Å, and 1.82 Å, respectively. However, we found that the interaction between the water molecule and the heterogeneous catalysts occurs by the formation of a M-O bond between the oxygen atom of the water molecule and the transition metal cluster and an O$\cdots$H bond between the hydrogen atom of water and the oxygen atom of closest silanol silica group. The equilibrium d_{M-O} distance are found to be 2.09 Å, 2.02 Å, 1.99 Å, and 2.02 Å for H_2O/(Fe_{13}@silica, Co_{13}@silica, Ni_{13}@silica, and Cu_{13}@silica), respectively, while those of O$\cdots$H bonds, are 1.66 Å, 1.51 Å, 1.64 Å, and 1.69 Å, respectively.

4. Discussion

4.1. Comparison between pure silica and M_{13} silica surfaces

Figure 5 shows the computed PBE+U+D2 adsorption energies of the most favorable structures for the guaiacol, catechol, anisole, phenol, CO, or H_2O molecules on different M_{13}@silica catalysts and on pure silica surface. We found that the adsorption energy depend on the type of the adsorbed molecule and the heterogeneous catalyst. The adsorption energies of the guaiacol and the catechol molecules are quite similar regardless the type of the silica catalyst. On pure silica surface, these energies are much larger than those of the other molecules, while on supported silica, are slightly lower.

Our results show that the guaiacol and catechol molecules are strongly bonded to the Ni_{13}@silica with an energy value of -284 kJ·mol^{-1}, which are 22 and 41 kJ·mol^{-1} lower

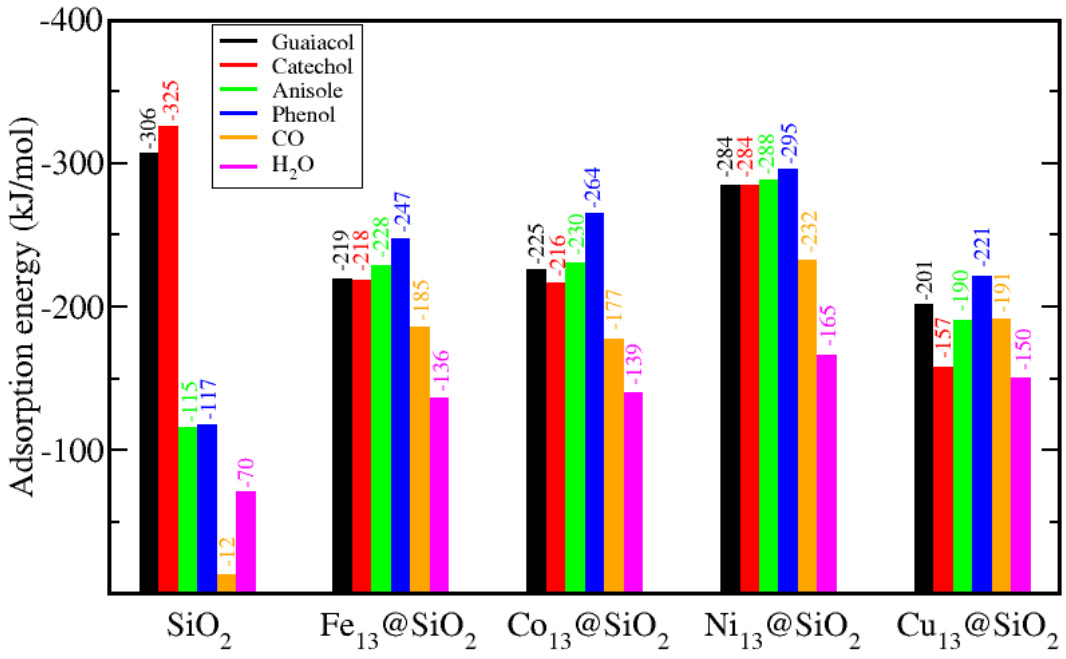

Figure 5: PBE+U+D2 computed ΔE_2 of the most favorable adsorption configurations of the phenolic compounds and the inhibiting molecules on pure silica surface and the different heterogeneous M_{13}@silica support.

compared to the pure silica surface. For Fe_{13}@silica, Co_{13}@silica, and Cu_{13}@silica catalysts, the adsorption energies of the guaiacol are found to be -219 and -225 and -201 kJ·mol^{-1}, respectively, while for catechol molecule, they are -218, -216, and -157 kJ·mol^{-1}, respectively.

In the case of the anisole molecule, the energy values are found to be -228, -230, -288, and -190 kJ·mol^{-1} for Fe_{13}, Co_{13}, Ni_{13}, and Cu_{13}@catalysts, respectively. These energy values are 113, 115, 173, and 75 kJ·mol^{-1} higher than those found on pure silica surface. Our results show also that the phenol is strongly bonded to Ni atoms of the Ni_{13}@silica interface with an energy value of -295 kJ·mol^{-1}, which is 178 kJ·mol^{-1} higher than the pure silica surface ones. For Fe_{13}@silica and Co_{13}@silica catalysts, the computed ΔE_2 of the phenol are found to be -247 kJ·mol^{-1} and -264 kJ·mol^{-1}, which are also much higher than that on silica surface (-117 kJ·mol^{-1}) [19, 71]. However, ΔE_2 of phenol on Cu_{13}@silica is of -221 kJ·mol^{-1}, which is 74 kJ·mol^{-1} lower than that on Ni_{13}@silica catalyst but still higher than the one on the pure silica surface. We found that the phenol and anisole molecules prefer to accommodate at the interface of the heterogeneous catalysts.

The calculated adsorption energies reported in Figure 5 show that the adsorption energy order for the different heterogeneous catalysts M_{13}@silica is: phenol > anisole > guaiacol > catechol, while for pure silica surface, is catechol > guaiacol > phenol > anisole. At

the interface, phenol and anisole are more stable than catechol and guaiacol, while the guaiacol and the catechol are the most stable ones on pure silica surface due to the strong hybridization between them which results a reorganization of the surface and a chemical modification of the molecules. However, the adsorption energy order for all the phenolic compounds is: Ni_{13}@silica > Co_{13}@silica > Fe $_{13}$@silica $\gg$ Cu_{13}@silica. This is mainly due to the deformation of the copper cluster which limits the number of interactions with the oxygenated molecules compared to the other clusters (see tables S5, S6, S7 and S8 in the supporting information). However, the nickel cluster has maximum interaction bonds with the different phenolic molecules.

4.2. Inhibiting effects

The adsorption energies of the most favorable configurations of inhibiting molecules on silica surface and heterogeneous catalysts are gathered in Figure 5. For pure silica surface, we found that the anisole and the phenol are the least adsorbed phenolic molecules with ΔE_2 of -115 and -117 kJ·mol^{-1}, respectively. The water molecule presents a ΔE_2 of -70 kJ·mol^{-1}, which is 45 kJ·mol^{-1} lower in absolute value than that of the anisole molecule, while for CO, ΔE_2 is found to be -12 kJ·mol^{-1}, which is -103 kJ·mol^{-1} lower in absolute value than the anisole adsorption value. This means that the pure silica support allows a selective adsorption of all the oxygenated molecules towards the typical byproducts of HDO, CO and H_2O.

For Fe_{13}@silica catalyst, the ΔE_2 of the phenolic compounds range between -218 and -247 kJ·mol^{-1}. In contrast, those of CO and H_2O molecules are -185 and -136 kJ·mol^{-1}, respectively, which make CO and H_2O less adsorbed than catechol by 33 and 82 kJ·mol^{-1}, respectively . This suggests that the adsorption of the oxygenated molecules is not impacted by the presence of inhibiting molecules on Fe_{13}@silica catalyst.

For Co_{13}@silica, the adsorption energies of phenolics range between -216 and -264 kJ·mol^{-1}, which are at least 39 and 77 kJ·mol^{-1} lower than those of CO and water molecules. This suggest that Co_{13}@silica will allow a selective adsorption of all phenolic compounds compared to inhibiting ones.

We found that the phenolic compounds strongly interact with Ni_{13}@silica catalyst with ΔE_2 of -284 kJ·mol^{-1} for guaiacol and catechol, -288 kJ·mol^{-1} for anisole, -295 kJ·mol^{-1} for phenol, compared to -232 kJ·mol^{-1} for CO, and -165 kJ·mol^{-1} for water molecule. Therefore, the inhibitory effect of CO and water on Ni_{13}@silica catalyst is negligible with a ΔE_2 of 52 and 119 kJ·mol^{-1} lower than those of the phenolic compounds.

These results suggest that the inhibitory effect of water and CO is negligible and therefore the heterogeneous catalysts materials (Fe_{13}@silica, Co_{13}@silica, and Ni_{13}@silica) are promising for the HDO process.

However, for Cu_{13}@silica, the ΔE_2 of the adsorbed CO and H_2O molecules are found to be -191 and -150 kJ·mol^{-1}, respectively, while that of the catechol molecule is of -157 kJ·mol^{-1}. Our results suggest that, for Cu_{13}@silica, water and CO are expected to be major inhibitors of the HDO process. We have to put these results in perspective with the evaluation of inhibiting effect of H_2O, H_2S or CO on HDO process using the conventional sulfide catalysts [25, 15, 72]. In particular, DFT calculations have shown that H_2O, H_2S

and CO are more strongly adsorbed than guaiacol and derivatives over MoS_2 and CoMoS surfaces under HDO conditions. The effect of water and H_2S are quite similar while CO is even more adsorbed, demonstrating that CO will be a major inhibitor of the HDO process of real feeds. These theoretical results have been then confirmed by experimental studies. A strong inhibiting effect of carbon monoxide (more than water) has been observed for sulfided $CoMo/Al_2O_3$ catalysts on the hydrodesulfurization reaction of 2-methylthiophene and hydrogenation of 2,3-dimethylbut-2-ene [72]. For HDO, Bouvier et al. [15] showed also that CO could inhibit the reactivity of 2-ethylphenol over MoS_2 and CoMoS phases supported on alumina while this effect was limited for NiMoS. Indeed, silica-based catalysts appear clearly as an attractive option to sulfide catalysts for HDO processing.

5. Conclusions

In this work, we have studied the interaction between a selection of phenolic compounds, potential inhibiting molecules H_2O and CO present in HDO feeds and different M_{13}@silica-3.3 catalysts (M = Fe, Co, Ni, and Cu) using density functional theory calculations. Different geometrical configurations were investigated systematically by means of the PBE+U+D2 approximation for guaiacol, catechol, anisole, phenol, CO, and H_2O adsorbed onto pure and supported M_{13} silica surface at different locations (support, cluster, and support/cluster interface) and for different orientations of the molecules ($O^{\perp}$, $O^{\parallel}$, $\pi^{\parallel}$). Our results show that the phenolics are strongly adsorbed whatever the heterogeneous catalysts. By comparing the resulting adsorption energies of the oxygenated compounds, we found that the Ni_{13}@silica catalyst offers the best affinity for phenolics, followed by Co_{13}@silica and Fe_{13}@silica, and then Cu_{13}@silica. Also, the adsorption energy order for the different heterogeneous catalysts M_{13}@silica is: phenol > anisole > guaiacol > catechol, while for the pure silica surface, is catechol > guaiacol > phenol > anisole. In all cases, the interaction energies of the phenol on the heterogeneous catalysts are more than 100 $kJ{\cdot}mol^{-1}$ higher than that on the pure silica surface. This shows that heterogeneous catalysts improve outstandingly the catalytic activity and selectivity. However, a very high interaction energy is found for guaiacol and catechol molecules on pure silica surface of -306 $kJ{\cdot}mol^{-1}$ and -325 $kJ{\cdot}mol^{-1}$, respectively, due to the strong Si-C interaction which results in a strong deformation of their aromatic-ring and reorganizations of the silica surface. We have shown that the inhibitory effect (CO and water molecules) on the oxygenated compounds adsorption are negligible for Fe_{13}@silica, Co_{13}@silica and Ni_{13}@silica catalysts, while for Cu_{13}@silica, they are expected to be major inhibitors of the HDO process. In conclusion, supported transition-metal (Fe, Co, Ni) clusters appear as suitable candidates for the HDO process based on the present investigation of this first adsorption step. Further studies may explore the catalytic reactivity of these promising silica materials.

Acknowledgments

We would like to gratefully acknowledge Pr. Mohammed Bettahar for fruitful discussions. This work was performed using the Lorraine University HPC Mesocenter "Explor"

and TGCC under the allocation 2021-A0100810433 by GENCI-EDARI . The authors are grateful to the program Lorraine University of Excellence for funding this work with the Lignin program. SG, SL and MB also acknowledge financial support through the COMETE project (COnception in silico de Matriaux pour l'EnvironmenT et l'Energie) cofunded by the European Union under the program "FEDER-FSE Lorraine et Massif des Vosges 2014-2020".

References

[1] A. J. Ragauskas, G. T. Beckham, M. J. Biddy, R. Chandra, F. Chen, M. F. Davis, B. H. Davison, R. A. Dixon, P. Gilna, M. Keller, P. Langan, A. K. Naskar, J. N. Saddler, T. J. Tschaplinski, G. A. Tuskan, C. E. Wyman, Lignin valorization: Improving lignin processing in the biorefinery, Science 344 (2014) 1246843. doi:10.1126/science.1246843.

[2] J. Zakzeski, P. C. A. Bruijnincx, A. L. Jongerius, B. M. Weckhuysen, The catalytic valorization of lignin for the production of renewable chemicals, Chem. Rev. 110 (6) (2010) 3552–3599. doi:10.1021/cr900354u.

[3] J. C. del Río, J. Rencoret, A. Gutiérrez, T. Elder, H. Kim, J. Ralph, Lignin monomers from beyond the canonical monolignol biosynthetic pathway: Another brick in the wall, ACS Sustain. Chem. Eng. 8 (13) (2020) 4997–5012. doi:10.1021/acssuschemeng.0c01109.

[4] E. Terrell, V. Carré, A. Dufour, F. Aubriet, Y. Le Brech, M. Garcia-Pérez, Contributions to lignomics: Stochastic generation of oligomeric lignin structures for interpretation of maldi-ft-icr-ms results, ChemSusChem 13 (17) (2020) 4428–4445. doi:10.1002/cssc.202000239.

[5] E. Terrell, L. D. Dellon, A. Dufour, E. Bartolomei, L. J. Broadbelt, M. Garcia-Perez, A review on lignin liquefaction: Advanced characterization of structure and microkinetic modeling, Ind. Eng. Chem. Res. 59 (2) (2020) 526–555. doi:10.1021/acs.iecr.9b05744.

[6] D. Nowakowski, A. Bridgwater, D. Elliott, D. Meier, P. de Wild, Lignin fast pyrolysis: Results from an international collaboration, J. Anal. Appl. Pyrolysis 88 (1) (2010) 53–72. doi:10.1016/j.jaap.2010.02.009.

[7] S. J. Hurff, M. T. Klein, Reaction pathway analysis of thermal and catalytic lignin fragmentation by use of model compounds, Ind. Eng. Chem. 22 (4) (1983) 426–430. doi:10.1021/i100012a012.

[8] M. Saidi, F. Samimi, D. Karimipourfard, T. Nimmanwudipong, B. C. Gates, M. R. Rahimpour, Upgrading of lignin-derived bio-oils by catalytic hydrodeoxygenation, Energy Environ. Sci. 7 (2014) 103–129. doi:10.1039/C3EE43081B.

[9] R. Olcese, M. Bettahar, D. Petitjean, B. Malaman, F. Giovanella, A. Dufour, Gas-phase hydrodeoxygenation of guaiacol over Fe/SiO_2 catalyst, Appl. Catal. B: Environ. 115-116 (2012) 63 – 73". doi:10.1016/j.apcatb.2011.12.005.

[10] R. N. Olcese, J. Francois, M. M. Bettahar, D. Petitjean, A. Dufour, Hydrodeoxygenation of guaiacol, a surrogate of lignin pyrolysis vapors, over iron based catalysts: Kinetics and modeling of the lignin to aromatics integrated process, Energy Fuels 27 (2) (2013) 975–984. doi:10.1021/ef301971a.

[11] R. N. Olcese, G. Lardier, M. Bettahar, J. Ghanbaja, S. Fontana, V. Carré, F. Aubriet, D. Petitjean, A. Dufour, Aromatic chemicals by iron-catalyzed hydrotreatment of lignin pyrolysis vapor, ChemSusChem 6 (8) (2013) 1490–1499. doi:10.1002/cssc.201300191.

[12] C. R. Lee, J. S. Yoon, Y.-W. Suh, J.-W. Choi, J.-M. Ha, D. J. Suh, Y.-K. Park, Catalytic roles of metals and supports on hydrodeoxygenation of lignin monomer guaiacol, Catal. Commun. 17 (2012) 54–58. doi:10.1016/j.catcom.2011.10.011.

[13] M. A. González-Borja, D. E. Resasco, Anisole and guaiacol hydrodeoxygenation over monolithic pt-sn catalysts, Energy & Fuels 25 (9) (2011) 4155–4162. doi:10.1021/ef200728r.

[14] G. Fogassy, C. Lorentz, G. Toussaint, N. Thegarid, Y. Schuurman, C. Mirodatos, Analytical techniques tailored for biomass transformation to biofuels, Environ. Prog. Sustain. Energy 32 (2) (2013) 377–383. doi:10.1002/ep.10631.

[15] C. Bouvier, Y. Romero, F. Richard, S. Brunet, Effect of h2s and co on the transformation of 2-ethylphenol as a model compound of bio-crude over sulfided mo-based catalysts: propositions of promoted active sites for deoxygenation pathways based on an experimental study, Green Chem. 13 (2011) 2441–2451. doi:10.1039/C1GC15181A.

[16] M. Bertero, G. de la Puente, U. Sedran, Fuels from bio-oils: Bio-oil production from different residual sources, characterization and thermal conditioning, Fuel 95 (2012) 263 – 271. doi:10.1016/j.fuel.2011.08.041.

[17] I. Graca, J. Lopes, M. Ribeiro, M. Badawi, S. Laforge, P. Magnoux, F. R. Ribeiro, n-heptane cracking over mixtures of hy and hzsm-5 zeolites: Influence of the presence of phenol, Fuel 94 (2012) 571 – 577. doi:10.1016/j.fuel.2011.11.033.

[18] J. Marsman, J. Wildschut, P. Evers, S. de Koning, H. Heeres, Identification and classification of components in flash pyrolysis oil and hydrodeoxygenated oils by two-dimensional gas chromatography and time-of-flight mass spectrometry, J. Chromatogr. A 1188 (1) (2008) 17–25. doi:10.1016/j.chroma.2008.02.034.

[19] Y. Berro, S. Gueddida, S. Lebègue, A. Pasc, N. Canilho, M. Kassir, F. E. H. Hassan, M. Badawi, Atomistic description of phenol, co and h2o adsorption over crystalline and amorphous silica surfaces for hydrodeoxygenation applications, Appl. Surf. Sci. 494 (2019) 721 – 730. doi:10.1016/j.apsusc.2019.07.216.

[20] H. Weigold, Behaviour of co-mo-al2o3 catalysts in the hydrodeoxygenation of phenols, Fuel 61 (10) (1982) 1021 – 1026, international Workshop on the 'Science of Coal Liquefaction'. doi:10.1016/0016-2361(82)90104-1.

[21] C. Bouvier, Y. Romero, F. Richard, S. Brunet, Effect of h2s and co on the transformation of 2-ethylphenol as a model compound of bio-crude over sulfided mo-based catalysts: propositions of promoted active sites for deoxygenation pathways based on an experimental study, Green Chem. 13 (2011) 2441–2451. doi:10.1039/C1GC15181A.

[22] V. N. Bui, D. Laurenti, P. Afanasiev, C. Geantet, Hydrodeoxygenation of guaiacol with como catalysts. part i: Promoting effect of cobalt on hdo selectivity and activity, Appl. Catal. B: Environ. 101 (3) (2011) 239 – 245. doi:10.1016/j.apcatb.2010.10.025.

[23] Y. Romero, F. Richard, S. Brunet, Hydrodeoxygenation of 2-ethylphenol as a model compound of bio-crude over sulfided mo-based catalysts: Promoting effect and reaction mechanism, Appl. Catal. B: Environ. 98 (3) (2010) 213 – 223. doi:10.1016/j.apcatb.2010.05.031.

[24] Q. Bu, H. Lei, A. H. Zacher, L. Wang, S. Ren, J. Liang, Y. Wei, Y. Liu, J. Tang, Q. Zhang, R. Ruan, A review of catalytic hydrodeoxygenation of lignin-derived phenols from biomass pyrolysis, Bioresour. Technol. 124 (2012) 470 – 477. doi:10.1016/j.biortech.2012.08.089.

[25] M. Badawi, J.-F. Paul, S. Cristol, E. Payen, Guaiacol derivatives and inhibiting species adsorption over mos2 and comos catalysts under hdo conditions: A dft study, Catal. Commun. 12 (10) (2011) 901 – 905. doi:10.1016/j.catcom.2011.02.010.

[26] D. C. Elliott, Historical developments in hydroprocessing bio-oils, Energy & Fuels 21 (3) (2007) 1792–1815. doi:10.1021/ef070044u.

[27] Q. Bu, H. Lei, A. H. Zacher, L. Wang, S. Ren, J. Liang, Y. Wei, Y. Liu, J. Tang, Q. Zhang, R. Ruan, A review of catalytic hydrodeoxygenation of lignin-derived phenols from biomass pyrolysis, Bioresour. Technol. 124 (2012) 470–477. doi:10.1016/j.biortech.2012.08.089.

[28] H. Zhao, D. Li, P. Bui, S. Oyama, Hydrodeoxygenation of guaiacol as model compound for pyrolysis oil on transition metal phosphide hydroprocessing catalysts, Appl. Catal. A: General 391 (1) (2011) 305–310. doi:10.1016/j.apcata.2010.07.039.

[29] E. Laurent, B. Delmon, Study of the hydrodeoxygenation of carbonyl, carboylic and guaiacyl groups over sulfided como/γ-al2o3 and nimo/γ-al2o3 catalyst: Ii. influence of water, ammonia and hydrogen sulfide, Appl. Catal. A: General 109 (1) (1994) 97–115. doi:10.1016/0926-860X(94)85005-4.

[30] E. Laurent, B. Delmon, Influence of water in the deactivation of a sulfided nimoγ-al2o3 catalyst during hydrodeoxygenation, J. Catal. 146 (1) (1994) 281–291. doi:10.1016/0021-9517(94)90032-9.

[31] M. Asadieraghi, W. M. Ashri Wan Daud, H. F. Abbas, Heterogeneous catalysts for advanced biofuel production through catalytic biomass pyrolysis vapor upgrading: a review, RSC Adv. 5 (2015)

22234–22255. doi:10.1039/C5RA00762C.
[32] S. De, B. Saha, R. Luque, Hydrodeoxygenation processes: Advances on catalytic transformations of biomass-derived platform chemicals into hydrocarbon fuels, Bioresour. Technol. 178 (2015) 108–118. doi:10.1016/j.biortech.2014.09.065.
[33] J. Wildschut, F. H. Mahfud, R. H. Venderbosch, H. J. Heeres, Hydrotreatment of fast pyrolysis oil using heterogeneous noble-metal catalysts, Ind. Eng. Chem. Res. 48 (23) (2009) 10324–10334. doi:10.1021/ie9006003.
[34] E. Furimsky, Catalytic hydrodeoxygenation, Appl. Catal. A: General 199 (2) (2000) 147–190. doi:10.1016/S0926-860X(99)00555-4.
[35] V. N. Bui, D. Laurenti, P. Afanasiev, C. Geantet, Hydrodeoxygenation of guaiacol with como catalysts. part i: Promoting effect of cobalt on hdo selectivity and activity, Appl. Catal. B Environ. 101 (3) (2011) 239–245. doi:10.1016/j.apcatb.2010.10.025.
[36] Y. Berro, S. Gueddida, Y. Bouizi, C. Bellouard, E.-E. Bendeif, A. Gansmuller, A. Celzard, V. Fierro, D. Ihiawakrim, O. Ersen, M. Kassir, F. E. H. Hassan, S. Lebegue, M. Badawi, N. Canilho, A. Pasc, Imprinting isolated single iron atoms onto mesoporous silica by templating with metallosurfactants, J. Colloid Interf. Sci. 573 (2020) 193 – 203. doi:10.1016/j.jcis.2020.03.095.
[37] H. Guesmi, R. Grybos, J. Handzlik, F. Tielens, Characterization of molybdenum monomeric oxide species supported on hydroxylated silica: a DFT study, Phys. Chem. Chem. Phys. 16 (2014) 18253–18260. doi:10.1039/C4CP02296C.
[38] M. Gierada, P. Michorczyk, F. Tielens, J. Handzlik, Reduction of chromia-silica catalysts: A molecular picture, J. Catal. 340 (2016) 122 – 135. doi:10.1016/j.jcat.2016.04.022.
[39] B. R. Goldsmith, B. Peters, J. K. Johnson, B. C. Gates, S. L. Scott, Beyond ordered materials: Understanding catalytic sites on amorphous solids, ACS Catal. 7 (11) (2017) 7543–7557. doi:10.1021/acscatal.7b01767.
[40] T. Siodla, I. Sobczak, M. Ziolek, F. Tielens, Theoretical and experimental insight into zinc loading on mesoporous silica, Micropor. Mesopor. Mat. 256 (2018) 199 – 205. doi:10.1016/j.micromeso.2017.08.008.
[41] F. Tielens, M. Gierada, J. Handzlik, M. Calatayud, Characterization of amorphous silica based catalysts using dft computational methods, Catal. Today 354 (2020) 3–18. doi:https://doi.org/10.1016/j.cattod.2019.03.062.
[42] C. Chizallet, P. Raybaud, Density functional theory simulations of complex catalytic materials in reactive environments: beyond the ideal surface at low coverage, Catal. Sci. Technol. 4 (2014) 2797–2813. doi:10.1039/C3CY00965C.
[43] S. Simonetti, A. D. Company, E. Pronsato, A. Juan, G. Brizuela, A. Lam, Density functional theory based-study of 5-fluorouracil adsorption on β-cristobalite (111) hydroxylated surface: The importance of H-bonding interactions, Appl. Surf. Sci. 359 (2015) 474 – 479. doi:10.1016/j.apsusc.2015.10.147.
[44] A. B. Schvval, A. Juan, G. F. Cabeza, Theoretical study of the role of the interface of Ag_4 nanoclusters deposited on TiO_2(110) and TiO_2(101), Appl. Surf. Sci. 490 (2019) 343 – 351. doi:10.1016/j.apsusc.2019.05.291.
[45] C. Ciotonea, I. Mazilu, B. Dragoi, C. Catrinescu, E. Dumitriu, A. Ungureanu, H. Alamdari, S. Petit, S. Royer, Confining for stability: Heterogeneous catalysis with Transition Metal (Oxide) Nanoparticles confined in the secondary pore network of mesoporous scaffolds, ChemNanoMat 3 (4) (2017) 233–237. doi:10.1002/cnma.201700014.
[46] C. Ciotonea, B. Dragoi, A. Ungureanu, C. Catrinescu, S. Petit, H. Alamdari, E. Marceau, E. Dumitriu, S. Royer, Improved dispersion of transition metals in mesoporous materials through a polymer-assisted melt infiltration method, Catal. Sci. Technol. 7 (2017) 5448–5456. doi:10.1039/C7CY00963A.
[47] B. Dragoi, I. Mazilu, A. Chirieac, C. Ciotonea, A. Ungureanu, E. Marceau, E. Dumitriu, S. Royer, Highly dispersed copper (oxide) nanoparticles prepared on SBA-15 partially occluded with the P123 surfactant: toward the design of active hydrogenation catalysts, Catal. Sci. Technol. 7 (2017) 5376–5385. doi:10.1039/C7CY01015J.
[48] S. Chen, C. Ciotonea, A. Ungureanu, E. Dumitriu, C. Catrinescu, R. Wojcieszak, F. Dumeignil, S. Royer, Preparation of nickel (oxide) nanoparticles confined in the secondary pore net-

work of mesoporous scaffolds using melt infiltration, Catal. Today 334 (2019) 48 – 58. doi:10.1016/j.cattod.2019.01.064.
[49] S. Gueddida, M. Badawi, S. Lebègue, Grafting of iron on amorphous silica surfaces from ab initio calculations, J. Chem. Phys. 152 (21) (2020) 214706. doi:10.1063/5.0007128.
[50] S. Gueddida, S. Lebègue, M. Badawi, Interaction between transition metals (co, ni, and cu) systems and amorphous silica surfaces: A dft investigation, Appl. Surf. Sci. 533 (2020) 147422. doi:10.1016/j.apsusc.2020.147422.
[51] G. Kresse, J. Furthmüller, Efficient iterative schemes for ab initio total-energy calculations using a plane-wave basis set, Phys. Rev. B 54 (1996) 11169–11186. doi:10.1103/PhysRevB.54.11169.
[52] P. E. Blöchl, Projector augmented-wave method, Phys. Rev. B 50 (1994) 17953–17979. doi:10.1103/PhysRevB.50.17953.
[53] J. P. Perdew, K. Burke, M. Ernzerhof, Generalized gradient approximation made simple, Phys. Rev. Lett. 77 (1996) 3865–3868. doi:10.1103/PhysRevLett.77.3865.
[54] S. Grimme, Semiempirical GGA-type density functional constructed with a long-range dispersion correction, J. Comput. Chem. 27 (15) (2006) 1787–1799. doi:10.1002/jcc.20495.
[55] T. Bucko, J. Hafner, S. Lebègue, J. G. Angyán, Improved description of the structure of molecular and layered crystals: Ab initio DFT calculations with van der Waals corrections, J. Phys. Chem. A 114 (43) (2010) 11814–11824. doi:10.1021/jp106469x.
[56] V. I. Anisimov, F. Aryasetiawan, A. I. Lichtenstein, First-principles calculations of the electronic structure and spectra of strongly correlated systems: the LDA+U method, J. Phys. Condens. Matter 9 (4) (1997) 767–808. doi:10.1088/0953-8984/9/4/002.
[57] O. Bengone, M. Alouani, P. Blöchl, J. Hugel, Implementation of the projector augmented-wave LDA+U method: Application to the electronic structure of nio, Phys. Rev. B 62 (2000) 16392–16401. doi:10.1103/PhysRevB.62.16392.
[58] W. Hu, L. Mei, H. Li, Simulation of ground state structure of nickel clusters (n $\leq$ 40), Solid State Commun. 100 (1996) 129 – 131. doi:10.1016/0038-1098(96)00396-1.
[59] M. Kabir, A. Mookerjee, A. K. Bhattacharya, Structure and stability of copper clusters: A tight-binding molecular dynamics study, Phys. Rev. A 69 (2004) 043203. doi:10.1103/PhysRevA.69.043203.
[60] Z. Xie, Q.-M. Ma, Y. Liu, Y.-C. Li, First-principles study of the stability and Jahn-Teller distortion of nickel clusters, Phys. Lett. A 342 (2005) 459 – 467. doi:10.1016/j.physleta.2005.05.067.
[61] G. R. S.D. Borisova, E. Chulkov, Structure and vibrational properties of cobalt clusters (n $\leq$ 20), Phys. Solid State 52 (2010) 838–843. doi:10.1134/S106378341004027X.
[62] E. Kim, A. Mohrland, P. F. Weck, T. Pang, K. R. Czerwinski, D. Tomànek, Magic numbers in small iron clusters: A first-principles study, Chem. Phys. Lett. 613 (2014) 59 – 63. doi:10.1016/j.cplett.2014.08.056.
[63] L. T. Zhuravlev, Concentration of hydroxyl groups on the surface of amorphous silicas, Langmuir 3 (3) (1987) 316–318. doi:10.1021/la00075a004.
[64] A. P. Legrand, The Surface Properties of Silicas, Wiley, 1998.
[65] J. L. Blin, C. Carteret, Investigation of the silanols groups of mesostructured silica prepared using a fluorinated surfactant: Influence of the hydrothermal temperature, J. Phys. Chem. C 111 (39) (2007) 14380–14388. doi:10.1021/jp072369h.
[66] F. Tielens, C. Gervais, J. F. Lambert, F. Mauri, D. Costa, Ab initio study of the hydroxylated surface of amorphous silica: A representative model, Chem. Mater. 20 (2008) 3336–3344. doi:10.1021/cm8001173.
[67] M. Gierada, I. Petit, J. Handzlik, F. Tielens, Hydration in silica based mesoporous materials: a DFT model, Phys. Chem. Chem. Phys. 18 (2016) 32962–32972. doi:10.1039/C6CP05460A.
[68] A. Comas-Vives, Amorphous SiO_2 surface models: energetics of the dehydroxylation process, strain, ab initio atomistic thermodynamics and IR spectroscopic signatures, Phys. Chem. Chem. Phys. 18 (2016) 7475–7482. doi:10.1039/C6CP00602G.
[69] C. H. Rochester, D.-A. Trebilco, Infrared study of the adsorption of phenols on silica immersed in heptane, J. Chem. Soc., Faraday Trans. 1 74 (1978) 1137–1145. doi:10.1039/F19787401137.
[70] A. Popov, E. Kondratieva, J. M. Goupil, L. Mariey, P. Bazin, J.-P. Gilson, F. Maugé, Bio-oils hydrodeoxygenation: Adsorption of phenolic molecules on oxidic catalyst supports, J. Phys. Chem. C

114 (37) (2010) 15661–15670. doi:10.1021/jp101949j.
[71] S. Gueddida, S. Lebègue, M. Badawi, Assessing the potential of amorphous silica surfaces for the removal of phenol from biofuel: A density functional theory investigation, J. Phys. Chem. C 124 (37) (2020) 20262–20269. doi:10.1021/acs.jpcc.0c06581.
[72] F. Pelardy, A. Daudin, E. Devers, C. Dupont, P. Raybaud, S. Brunet, Deep hds of fcc gasoline over alumina supported comos catalyst: Inhibiting effects of carbon monoxide and water, Applied Catalysis B: Environmental 183 (2016) 317–327. doi:https://doi.org/10.1016/j.apcatb.2015.10.026.